Thermochimica Acta 498 (2010) 117–123

Contents lists available at ScienceDirect

Thermochimica Acta

journal homepage: www.elsevier.com/locate/tca

Fast cure kinetics of a UV-curable resin for UV nano-imprint lithography: Phenomenological model determination based on differential photocalorimetry results

Woo-Song Kim, Kyung-Seo Park, Jin Hyun Nam*, Donghoon Shin, Siyoul Jang, Tae-Yong Chung

School of Mechanical and Automotive Engineering, Kookmin University, 861-1 Jeongneung-dong, Seongbuk-gu, Seoul 136-702, Republic of Korea

ARTICLE INFO

Article history:
Received 5 August 2009
Received in revised form 6 October 2009
Accepted 14 October 2009
Available online 23 October 2009

Keywords:
UV-curable resin
Cure kinetic model
Nano-imprint lithography
Differential scanning calorimetry
Differential photocalorimetry
Parameter estimation

ABSTRACT

The fast cure kinetics of an ultraviolet (UV) light-curable resin for UV nano-imprint lithography (UV-NIL) was measured using a differential photocalorimeter (DPC). A simple phenomenological model was formulated to describe the curing behaviors of the UV-curable resin, i.e., the initial fast reaction rate at a small degree of cure and the autocatalytic reaction rate at a larger degree of cure. Kinetic model parameters were best fitted to the measured cure rate by using an error minimization technique. The practical applicability of the phenomenological model developed herein was demonstrated by a good agreement between the measured and modeled curing behaviors of the UV-curable resin. The effect of cure conditions on the estimated kinetic model parameters was also investigated.

1. Introduction

Nano-imprint lithography (NIL) is a promising lithographic technology that is suitable for the mass-production of nano-sized resist patterns via relatively simple steps [1–3]. In NIL, a mold containing nano-structures is first pressed upon a thin polymer film applied to a substrate, thereby physically deforming the film. Next, an anisotropic etching process, such as reactive ion etching (RIE), is used to remove unwanted material, leaving nano-sized polymer resist patterns on the substrate [4]. In addition to the simplicity of the process, NIL has several advantages over other lithographic technologies, including high resolution, low cost, and high throughput. Extensive research is currently being conducted to improve NIL.

Thermoplastic materials, such as polymethylmethacrylate (PMMA), were initially used as the resist polymer film in NIL [5–7]. In the thermal NIL, the mold and substrate are heated above the glass transition temperature, T_g, such that nano-sized patterns can be press-molded into the thermoplastic film. Once the film has been patterned, the film is then cooled below T_g in order to obtain rigid structures. Note that PMMA has a relatively high T_g of about 100 °C. Thus, NIL based on PMMA as a resist material requires high temperatures (around 150–200 °C) and good temperature control (i.e. the scheduled heating/cooling of the mold and substrate) for successful pattern transfer. Recently, alternative polymer resist materials, such as ultraviolet (UV) light-curable resins [8], have been proposed for use in NIL.

NIL based on UV-curable resins (UV-NIL) [9] utilizes simpler processes and equipment than thermal NIL based on thermoplastic materials. Note that UV-NIL is also called step-and-flash imprint lithography (SFIL) [10]. UV-NIL is performed at isothermal conditions near room temperature and does not require the sophisticated temperature control essential to thermal NIL. In addition, very small forces are used to press the low viscosity resins in UV-NIL, which is advantageous for processing fragile substrates or patterning multilayer structures. The UV-curable resins for UV-NIL are required to have fast cure kinetics for high throughput, low viscosity for good moldability, low surface energy for easy mold release, high tensile strength for pattern integrity, low shrinkage for structural stability, and less volatile solvent for low environmental pressures [2,3].

The chemical and physical cure kinetics of UV-curable resins has been extensively studied due to their utility in a wide variety of applications, such as instantaneous coating, dental reconstruction, and rapid prototyping [11,12]. The cure kinetics of UV-curable resins has been experimentally measured using light spectroscopy and/or differential photocalorimetry (DPC) [13–19]. Light spectroscopy techniques measure the variation of light transmission properties of a resin, which is directly dependent on degree of cure, whereas DPC techniques measure the heat released from a resin due to polymerization, which is proportional to cure rate. Thus, DPC

* Corresponding author. Tel.: +82 2 910 4858; fax: +82 2 910 4839.
E-mail address: akko2@kookmin.ac.kr (J.H. Nam).

0040-6031/$ – see front matter © 2009 Elsevier B.V. All rights reserved.
doi:10.1016/j.tca.2009.10.011

enables a detailed investigation of curing behaviors due to its high sensitivity to cure rate; however, the aforementioned light spectroscopy techniques can also be useful for the *in situ* monitoring of degree of cure during actual processes.

In this study, the fast cure kinetics of a UV-curable resin for UV-NIL was investigated using a DPC technique. Without referring to the exact composition or chemical kinetics of the resin, a general phenomenological model was developed to describe the curing behaviors identified by DPC. The kinetic parameters for the phenomenological model were estimated through an error minimization technique. The practical applicability of the proposed model was verified by comparing the measured and modeled cure kinetics of the UV-curable resin. The dependences of kinetic model parameters on cure temperature and UV light intensity were also investigated.

2. Differential photocalorimetric measurement

2.1. Material and procedure

A UV-curable resin designed for UV-NIL was purchased from Minuta Technology Co. in Korea (MINS-OR-08). This resin is a transparent liquid with a slight yellow tint and exhibits a moderate viscosity. The physical properties of the resin are summarized in Table 1. The composition of the UV resin is specified as a mixture of multifunctional acrylate monomers, oligomers, a small concentration of photoinitiators, and additives. The wavelength range required for UV curing of the resin is specified as the UV-A band (310–400 nm).

The DPC for the UV-curable resin was conducted using a differential scanning calorimeter (DSC-Q1000, TA Instrument Co., Delaware, USA) with a photocalorimetry accessory (PCA). The PCA equipment produces 20,000 mW/cm^2 of UV light from a high-pressure mercury lamp (250–650 nm). The intensity and wavelength band of the UV light used to irradiate a sample for DSC can be modified using appropriate filter devices.

Approximately 4.0 mg of the UV-curable resin was spread uniformly in an open aluminum pan and placed inside the sample chamber of the DSC equipment. The sample was maintained at a prescribed cure temperature for 20 s before each measurement run started. Next, a UV light of prescribed intensity was irradiated to the sample and the heat released due to the polymerization of the resin was recorded at a sampling rate of 20 Hz. Each measurement run was conducted at a prescribed cure temperature (isothermal mode) within a nitrogen rich environment for two minutes.

Two series of measurement runs were performed to investigate the effects of cure temperature (series 1) and UV intensity (series 2) on cure kinetics. In measurement series 1, the cure temperature, T_c, was set at 15, 25, 35, and 45 °C at a constant intensity of UV light irradiation, I_{uv}, of 13 mW/cm^2. In measurement series 2, the intensity of UV light irradiation was set at 6, 13, and 22 mW/cm^2 while the cure temperature was fixed at 25 °C. The standard condition of T_c = 25 °C and I_{uv} = 13 mW/cm^2 was common to both measurement series 1 and 2.

Table 1
Physical properties of the UV-curable resin (MINS-OR-08, Minuta Technology Co., Korea).

Properties	Unit	Specification
Appearance	–	Clear liquid
Color	Gardner	3.4
Viscosity @ 25 °C	cP	11.6
Refractive index (liquid)	–	1.4813
Density @ 25 °C	g/cm^3	1.0676

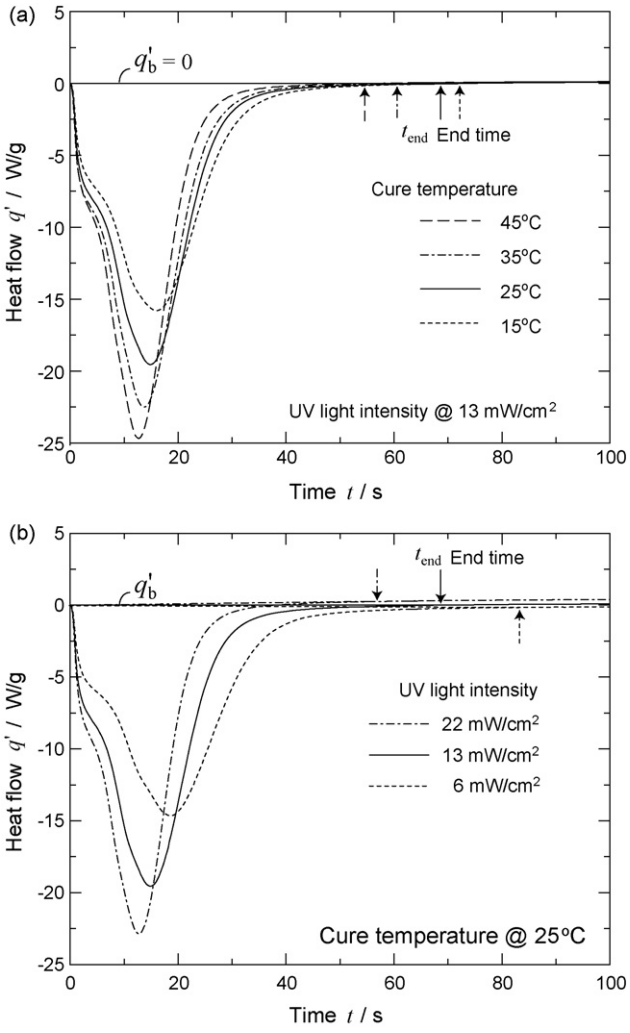

Fig. 1. Heat flow, q', measured by DPC: (a) series 1 variation of cure temperature, T_c, and (b) series 2 variation of UV light intensity, I_{uv}.

2.2. Measured heat flow

Because monomers lose their energy when they fit into cross-linked polymer structures, the heat flow measured during polymerization is well related to the reduction of the monomer concentration, i.e. the progress of cure. Fig. 1 shows the mass-specific heat flow, q' (W/g), measured by DPC. Each heat flow curve was slightly moved to align its starting point to the origin of the coordinate (q' = 0 at t = 0).

In Fig. 1, the polymerization of the UV-curable resin seems to be completed within a short time of about 60–80 s irrespective of the cure conditions considered in this study. Fig. 1 also indicates that a higher cure temperature or a higher intensity of UV light results in a faster polymerization rate with an increase in the peak heat flow. A deflection point is always observed at an earlier time in each heat flow curve. This behavior is believed to be caused by the fast initial polymerization rate.

A quantitative summary of the DPC measurement is provided in Table 2. The peak time, t_{peak}, denotes the instance at which a heat flow curve reaches its maximum. Similarly, the end time, t_{end}, denotes the instance at which the measured heat flow returns to zero at the completion of polymerization. While t_{peak} is easily discernible in Fig. 1, t_{end} is not, especially for the heat flow curves shown in Fig. 1(b). For some reason, the heat flow measured for I_{uv} of 6 or 22 mW/cm^2 has a non-zero asymptote as $t \to \infty$. Alter-

Table 2
Summary of DPC measurements of the UV-curable resin (MINS-OR-08, Minuta Technology Co., Korea).

Runs no.	Cure temperature T_c (°C)	UV light intensity I_{uv} (mW/cm^2)	Reaction heat Δh_p (J/g)	Temperature rise ΔT_r (°C)	Peak time t_{peak} (s)	End time t_{end} (s)
Series 1	15	13	−316.6	5.11	16.0	72.2
	25		−340.1	5.95	14.9	68.7
	35		−354.5	7.16	13.7	60.6
	45		−342.1	7.13	12.7	54.6
Series 2		6	−328.1	4.69	18.6	83.3[a]
	25	13	−340.1	5.69	14.9	68.7
		22	−319.2	7.13	12.7	56.9[a]

[a] These end times were estimated with a linear correlation of $t_{end} = 4.48 t_{peak}$ ($R^2 = 0.948$) determined for measurement series 1.

natively, for an I_{uv} of 6 or 22 mW/cm^2, t_{end} was estimated based on a linear correlation of $t_{end} = 4.48\ t_{peak}$ ($r^2 = 0.948$) that had been determined from measurement series 1.

Although DPC was performed in an isothermal mode at a prescribed cure temperature, the sample temperature was found to change considerably during measurement, as indicated by a maximum temperature rise, ΔT_r, of about 5–7 °C in Table 2. It should be noted that this temperature rise is generally unavoidable in DPC; however, the reaction heat absorbed by the resin during such temperature variation is expected to be small considering that the specific heat of acrylate resins are about 2 J/g K and about 1 J/g K for their polymer forms.

The total reaction heat of polymerization, Δh_p, listed in Table 2 was calculated as

$$\Delta h_p = \int_0^{\infty} q'_c(t^*)\,dt^* \approx \int_0^{t_{end}} q'_c(t^*)\ dt^*, \tag{1}$$

where t^* is the integration variable. Eq. (1) uses the corrected mass-specific heat flow, q'_c, to reduce the error caused by the non-zero asymptotic value of q' at $t \to \infty$. Thus, q'_c was defined as

$$q'_c(t) = q'(t) - q'_b(t), \tag{2}$$

where q'_b is the base heat flow that linearly connects the starting and ending heat flow data points ($q' = 0$ at $t = 0$ and $q' = q'_{end}$ at $t = t_{end}$). This base heat flow is also indicated in Fig. 1(b).

The average value of Δh_p was measured to be about -334.4 ± 20 J/g with an error range of ±6%. Note that the uncertainty from the microbalance used in weighing the resin samples was estimated to be about ±1.25% (±0.05 mg/4.0 mg).

2.3. Curing behavior

Two basic assumptions were used to convert the corrected heat flow, q'_c, into degree of cure, α, or cure rate, $\alpha'(\equiv d\alpha/dt)$. First, most of the measured heat flow originates from monomers upon cross-linking. Second, monomer concentration at the end of each measurement approaches zero. With these two assumptions, cure rate, α', could be directly determined as [16,18,19]

$$\alpha'(t) = \frac{q'_c(t)}{\Delta h_p}. \tag{3}$$

The instantaneous degree of cure, $\alpha(t)$, was then determined by integrating the cure rate as

$$\alpha(t) = \int_0^t \alpha'(t^*)\ dt^* = \int_0^t \frac{q'_c(t^*)\,dt^*}{\Delta h_p}. \tag{4}$$

In Table 2, Δh_p has relatively similar values for all measurement runs and also shows no obvious trend with respect to cure temperature or UV light intensity. Thus, the resin seems to reach a similar final degree of cure attainable for the cure conditions considered in this study. It should be noted that the above equations still produce meaningful results when the second assumption is violated by having a non-zero monomer concentration at the end of the measurement. In such cases, the degree of cure, α, determined by Eqs. (3) and (4) can be viewed as a relative degree of cure that is normalized by the final degree of cure. Light spectroscopy can be used to determine the final degree of cure on an absolute scale.

Fig. 2 shows the histories of cure rate and degree of cure determined for the standard condition of 25 °C and 13 mW/cm^2. Note the close resemblance between q' in Fig. 1 and α' in Fig. 2 according to Eq. (3). Fig. 2 indicates that the degree of cure initially increases rather fast with high cure rates. The maximum cure rate, α'_{max}, is observed to occur when the degree of cure is about 0.5. After that instance, the cure rate decreases, thereby reducing the slope in the α curve. The deflection point that is evident in the α' curve is not noticeable in the α curve because of integration.

Inspecting the phase plot of cure rate vs. degree of cure is a good way to investigate the cure kinetics of polymerization reactions. The α–α' plot for the standard condition is presented in Fig. 3. It is observed that a phenomenological autocatalytic rate equation, $\alpha'_{ac} = k_\alpha \alpha(1-\alpha)$, well describes the curing behavior of the UV-curable resin for the later part of polymerization ($\alpha > 0.2$). The curing behavior of the resin, which deviates from the autocatalytic rate equation, is identified by subtracting α'_{ac} from the experimentally determined α'. The initial part of the deviation is denoted as α'_{pi} in Fig. 3. It is observed that α'_{pi} grows very fast and then decays rather fast as α increases, leading to a negligible contribution of α'_{pi} to α' for $\alpha > 0.2$.

Similar α–α' curves were previously obtained for UV-curable resins for SFIL processes [20–22]. Note that the asymmetry in the α–α' curve in Fig. 3 is caused by the fast initial reaction rate. Because $t_{end} \approx 4.5\ t_{peak}$, the locus for $\alpha < 0.5$ roughly corresponds to 18%

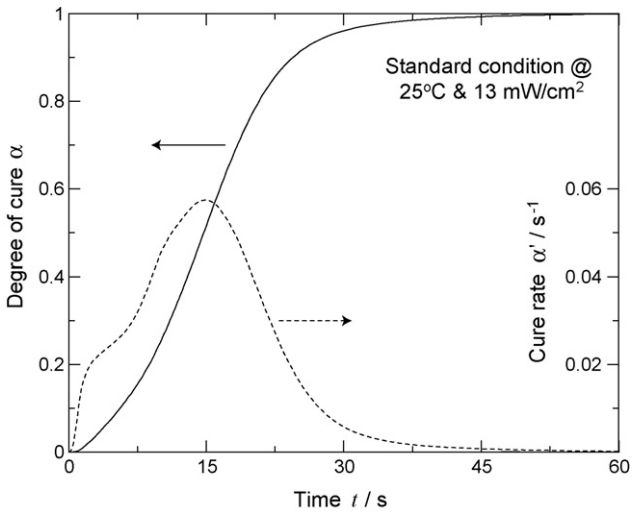

Fig. 2. Temporal evolution of cure rate, α', and degree of cure, α, for the standard condition of $T_c = 25$ °C and $I_{uv} = 13$ mW/cm^2.

(1/5.5) of the curing time, while that for $\alpha > 0.5$ corresponds to the remaining 82% (4.5/5.5).

3. Phenomenological kinetic model

3.1. Model description

A phenomenological kinetic model was formulated based on four elementary reaction steps for photoinitiated free-radical polymerizations [23], summarized as

$$I \xrightarrow{\text{UV}} 2R^{\bullet} \quad \text{(production of primary radicals)}, \tag{5}$$

$$R^{\bullet} + M \rightarrow RM^{\bullet} \quad \text{(initiationofchainradicals)}, \tag{6}$$

$$RM_n^{\bullet} + M \rightarrow RM_{n+1}^{\bullet} \quad \text{(propagationofthechain), and} \tag{7}$$

$$RM_n^{\bullet} + RM_m^{\bullet} \rightarrow \text{unreactivespecies} \quad \text{(terminationofthechain)}. \tag{8}$$

Here I is the photoinitiator that produces primary radicals, $R^{\bullet}$, upon exposure to UV light; M is the monomer; and $RM_n^{\bullet}$ is the chain radical.

With this four-step reaction mechanism in mind, the high polymerization rate for $\alpha < 0.2$ observed in Fig. 3 is naturally related to the initiation step of Eq. (6). The reaction rate of the initiation step is expected to be relatively high due to the high reactivity and mobility of primary radicals and also due to the abundance of monomers. Fig. 3 also shows that the polymerization rate for $\alpha > 0.2$ is well described by a phenomenological autocatalytic rate equation. This indicates that the propagation and termination steps of Eqs. (7) and (8) in near absence of primary radicals can be properly described by the autocatalytic rate equation, $\alpha'_{ac} = k_{\alpha}\alpha(1-\alpha)$.

Thus, this study focused on capturing the initial fast reaction by tracing the evolution of the photoinitiator and the primary radical concentration, while the reaction rate due to the propagation and termination steps was simply modeled using a phenomenological autocatalytic rate equation. Although simplified, this approach provided a phenomenological model for practical prediction of the curing behavior in UV-NIL processes.

The phenomenological kinetic model is composed of the following three rate equations. The first equation is for the photoinitiator concentration [I], written as

$$\frac{d\gamma}{dt} = -k_{\gamma}\gamma, \tag{9}$$

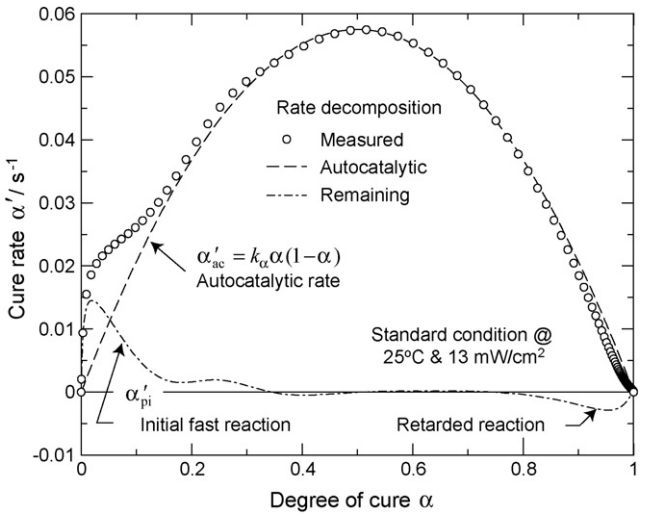

Fig. 3. Variation of cure rate, α', with respect to degree of cure, α, for the standard condition of $T_c = 25\,^{\circ}\text{C}$ and $I_{uv} = 13\,\text{mW/cm}^2$.

where γ is the normalized photoinitiator concentration, defined as $\gamma \equiv [I]/[I]^{\circ}$ (the superscript o denotes the initial concentration). Eq. (9) indicates that the photoinitiator concentration exponentially decays with a rate constant, k_{γ} (1/s). This is because the probability that a photoinitiator molecule is hit by UV photons and thus decomposes into primary radicals according to Eq. (5) is constant for a constant UV light intensity. The initial condition for γ should be 1 according to the definition of $\gamma \equiv [I]/[I]^{\circ}$.

The second rate equation in the phenomenological kinetic model is for the concentration of primary radicals [$R^{\bullet}$], expressed as

$$\frac{d\beta}{dt} = mk_{\gamma}\gamma - k_{\beta}\beta(1-\alpha), \tag{10}$$

where β is the normalized primary radical concentration, defined as $\beta \equiv [R^{\bullet}]/[M]^{\circ}$, and α is the degree of cure that is related to the monomer concentration [M], as $\alpha \equiv 1–[M]/[M]^{\circ}$. Primary radicals are produced by the decomposition of photoinitiators according to Eq. (5) and are consumed in the initiation step according to Eq. (6). The reaction rate of the initiation step is proportional to the concentration of primary radicals [$R^{\bullet}$], and that of monomers [M]. Eq. (10) indicates that the concentration of primary radicals increases at a production rate of $+mk_{\gamma}\gamma$ and the decreases at a consumption rate of $-k_{\beta}\beta(1-\alpha)$, where k_{β} (1/s) is a rate constant of β. The initial condition for β should be 0 because there are no primary radicals at the beginning.

It should be noted that the concentration of photoinitiators, γ, is normalized by the initial concentration of photoinitiators [I]°, while the concentration of primary radicals, β, is normalized by the initial concentration of monomers [M]°. Thus, a conversion factor of m is introduced in Eq. (10) to consider the different normalization of γ and β. When each primary radical combines with a monomer to produce a chain radical according to the initiation step described in Eq. (6), the conversion factor, m, can be exactly determined as $m = 2[I]^{\circ}/[M]^{\circ}$ for a resin with a fixed photoinitiator concentration; however, in this study, the conversion factor, m, was treated as a variable empirical parameter to fit the measured cure rate.

The final rate equation in the phenomenological kinetic model is for the concentration of monomers [M], written as

$$\frac{d\alpha}{dt} = k_{\beta}\beta(1-\alpha) + k_{\alpha}\alpha(1-\alpha), \tag{11}$$

where α is the degree of cure, defined as $\alpha \equiv 1 - [M]/[M]^{\circ}$. The first term in the right hand side of Eq. (11) is the monomer consumption rate due to the initiation step in Eq. (6) (α'_{pi} in Fig. 3). Similarly, the second term is the phenomenological autocatalytic rate that describes the propagation and the termination steps in Eqs. (7) and (8) (α'_{ac} in Fig. 3). Thus, k_{α} (1/s) is the autocatalytic rate constant. The initial condition for α should be 0 according to the definition of $\alpha \equiv 1 - [M]/[M]^{\circ}$.

3.2. Parameter estimation

The autocatalytic rate constant, k_{α}, can be determined by fitting $\alpha'_{ac} = k_{\alpha}\alpha(1-\alpha)$ to the α–α' curve ($\alpha > 0.2$) determined by DPC. In this study, a simpler approach was used to determine k_{α} as

$$k_{\alpha} = 4\alpha'_{max}, \tag{12}$$

where α'_{max} is the maximum cure rate determined experimentally. This approach is justified by the fact that the expression for α'_{ac} in Eq. (11) has a maximum of $0.25k_{\alpha}$ at $\alpha = 0.5$. Thus, k_{α} was considered to be a predetermined constant for the parameter estimation procedure explained below. A minutely modified autocatalytic rate equation, $\alpha'_{ac} = k_{\alpha}\alpha^{1+\delta}(1-\alpha)^{1-\delta}$, was also used in some cases.

Kinetic parameters of the phenomenological model were estimated by utilizing an optimization procedure. That is, k_{β}, k_{γ}, and

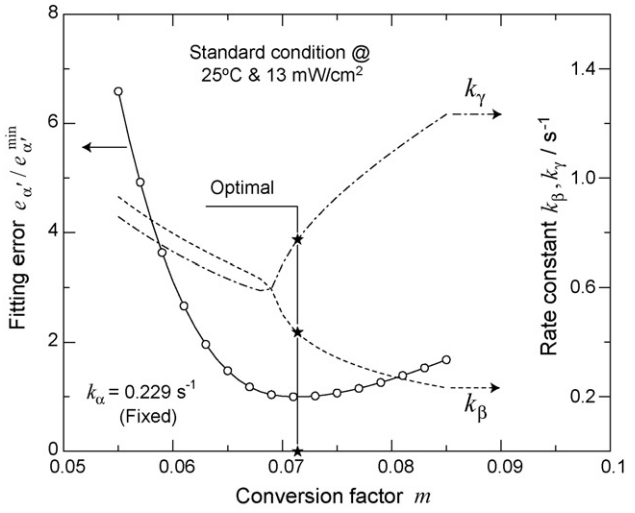

Fig. 4. Parameter estimation procedure based on error minimization for the standard condition of T_c = 25 °C and I_{uv} = 13 mW/cm².

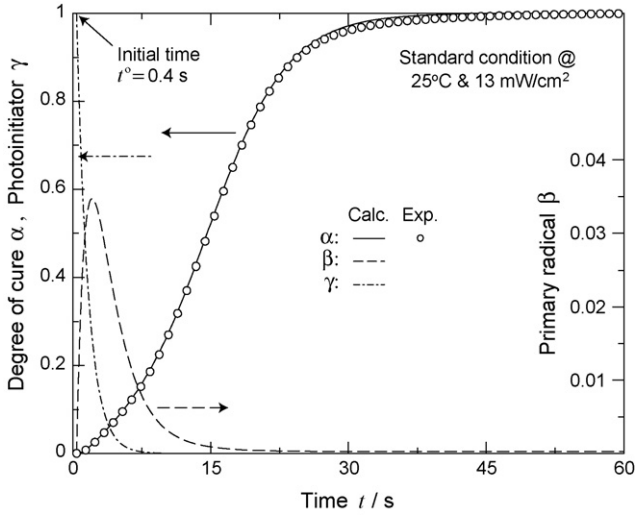

Fig. 5. Predicted temporal evolution of concentrations for the standard condition of T_c = 25 °C and I_{uv} = 13 mW/cm².

m were optimized to minimize the total square error, $e_{\alpha'}$, defined as

$$e_{\alpha'}(k_\beta, k_\gamma, m) = \int_0^{t_{end}} [\alpha'_{dpc}(t) - \alpha'_{mod}(t)]^2 \, dt, \quad (13)$$

where α'_{dpc} means the measured cure rate and α'_{mod} the predicted rate.

For the estimation of $e_{\alpha'}$, three rate equations of Eqs. (9)–(11) should be solved numerically. In this study, an explicit Euler method was employed for simplicity. In fact, the solution obtained by the Euler method showed no noticeable differences with that obtained by the fourth order Runge–Kutta method. The solution procedure based on the explicit Euler method was easily implemented using Excel™ spreadsheet software. In addition, parameter estimation was performed by utilizing the "solver" tool in Excel™ spreadsheet to minimize $e_{\alpha'}$.

The initial time, t°, was set as 0.4 s to compensate for the short delay time in DPC measurement. The measured heat flow during this period (0–0.4 s) showed a trend different from that just after the period, a difference believed to result from the thermal mass of certain devices in the DSC equipment. In addition, the degree of cure remained practically zero for this period. The time step for the Euler method was set as 0.05 s, which is consistent with the sampling interval used in DPC.

Fig. 4 explains the parameter estimation procedure performed for the standard condition of 25 °C and 13 mW/cm². As mentioned above, k_α was predetermined to be 0.229 s^{-1} before the parameter estimation procedure. In Fig. 4, the optimal values for k_β and k_γ with respect to the conversion factor, m, are shown along with the estimated total error, $e_{\alpha'}$. The optimal set of parameters, i.e. k_β, k_γ, and m, for the standard condition was determined by the minimum $e_{\alpha'}$, as illustrated in Fig. 4. The kinetic parameters estimated for all measurement runs are summarized in Table 3.

It should be noted that some uncertainty was inevitable in the optimization procedure. This is inferred by a relatively wide valley near the minimum of $e_{\alpha'}$ (the cost function) at m = 0.714 in Fig. 4. In fact, the k_β and k_γ determined for a slightly different value of m from the optimal was also found to describe the curing behavior relatively well. This is because the present parameter estimation procedure tries to fit only the cure rate, α', obtained by DPC. The uncertainty in the parameter estimation is expected to be reduced if additional data regarding the concentration of photoinitiators or of primary radicals are provided.

4. Results and discussion

Fig. 5 presents the histories of α, β, and γ that were calculated with the optimized kinetic parameters for the aforementioned standard condition. The initial time, t°, was set as 0.4 s to consider the delay time in the measurement. In Fig. 5, the normalized photoinitiator concentration, γ, decays very fast and becomes practically zero about eight seconds after UV light irradiation started. The normalized concentration of primary radicals, β, reaches its maximum shortly after the process began and decays rather slowly until about 25 s. The calculated degree of cure, α, seems to agree very well with the experimentally determined degree of cure.

The curing behaviors measured by DPC and those predicted by the phenomenological model are compared in Figs. 6 and 7, wherein it can be observed that the model describes the fast cure kinetics of the UV-curable resin very well. Thus, the practical appli-

Table 3
Kinetic model parameters estimated for the UV-curable resin (MINS-OR-08, Minuta Technology Co., Korea).

Runs no.	Cure temperature T_c (°C)	UV light intensity I_{uv} (mW/cm²)	m	k_α (s^{-1})	k_β (s^{-1})	k_γ (s^{-1})
Series 1	15	13	0.0952	0.198	0.235	0.943
	25		0.0714	0.229	0.435	0.773
	35		0.0652	0.251	0.504	0.871
	45		0.0565	0.287	0.741	0.719
Series 2	25	6	0.0738	0.178	0.309	0.724
		13	0.0714	0.229	0.435	0.773
		22	0.0747[a]	0.287	0.654[a]	0.637[a]

[a] These kinetic parameters were estimated with a modified autocatalytic reaction model of $\alpha'_{ac} = k_\alpha \alpha^{1+\delta}(1-\alpha)^{1-\delta}$ with δ = 0.038. Note that the modified equation for α'_{ac} has a maximum of 0.2504k_α at α = 0.52 (similar to the maximum of 0.25k_α at α = 0.5 in the original autocatalytic equation).

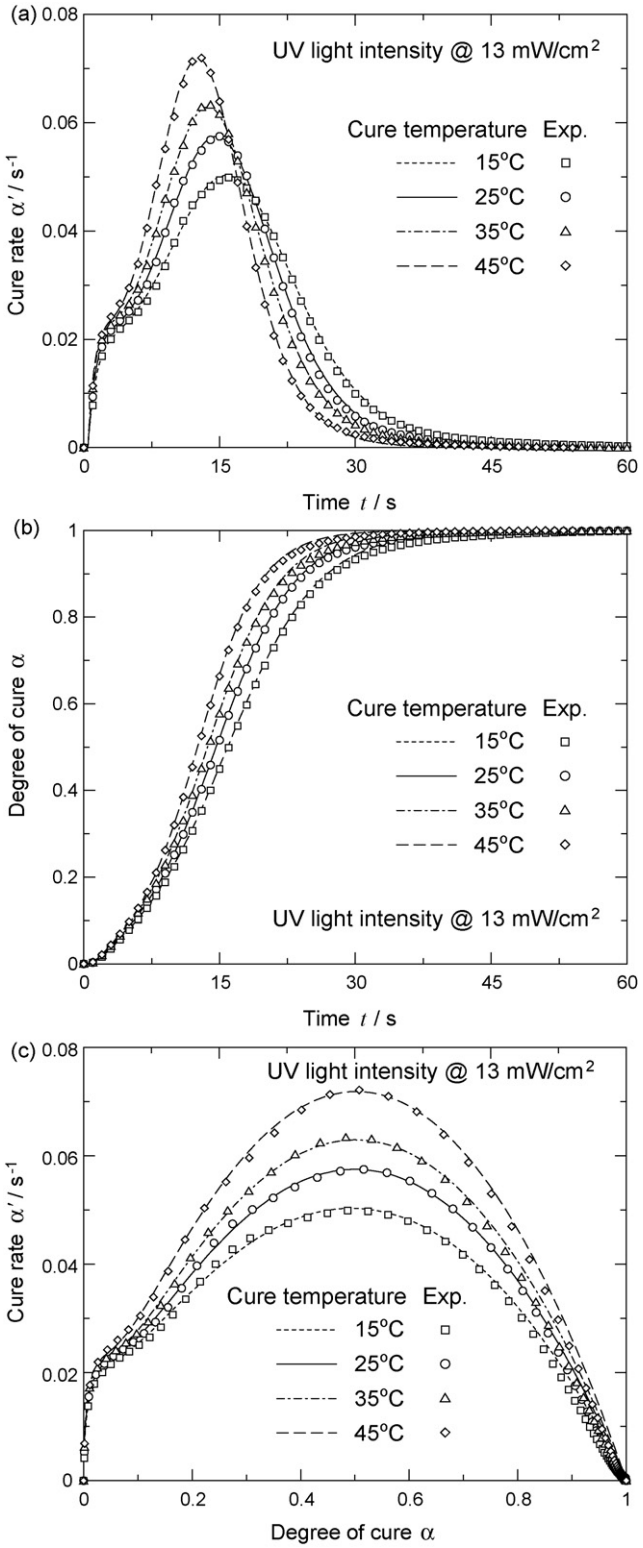

Fig. 6. Comparison of measured and predicted curing behavior of the resin for measurement series 1 variation of cure temperature, T_c: temporal evolution of (a) cure rate, α', and (b) degree of cure, α, and (c) plots of cure rate vs. degree of cure, α'–α.

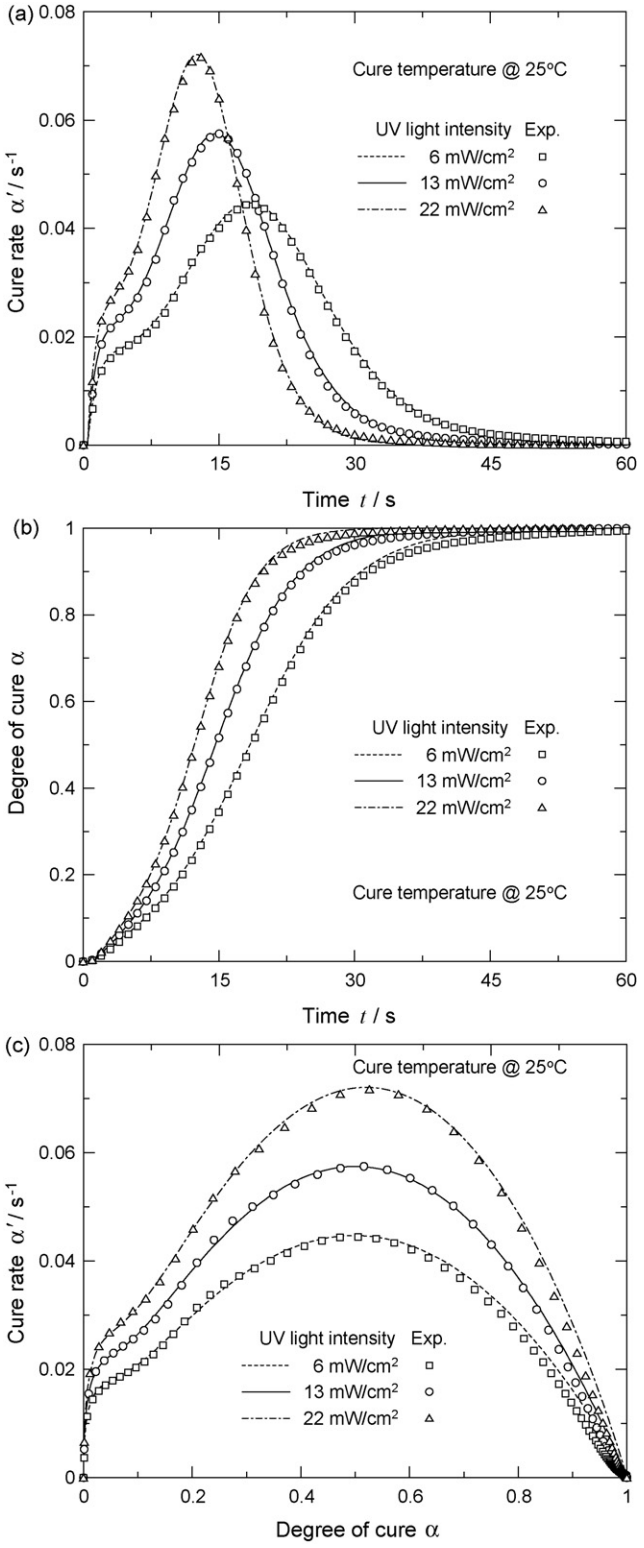

Fig. 7. Comparison of measured and predicted curing behavior of the resin for measurement series 2 variation of UV light intensity, I_{uv}: temporal evolution of (a) cure rate, α', and (b) degree of cure, α, and (c) plots of cure rate vs. degree of cure, α'–α.

cability of the present phenomenological model is partly verified by the results shown in Figs. 6 and 7. It should be noted that a modified autocatalytic rate equation, $\alpha'_{ac} = k_\alpha \alpha^{1+\delta}(1-\alpha)^{1-\delta}$ with $\delta = 0.038$, was used for the cure condition of 25 °C and 22 mW/cm^2 to better describe the curing behavior for $\alpha > 0.2$; however, the modified equation for α'_{ac} is only minutely different from the original equation by having a maximum of 0.2504 k_α at $\alpha = 0.52$ (comparable to the maximum of 0.25 k_α at $\alpha = 0.5$ in the original equation).

The effect of cure conditions on the estimated kinetic parameters is in Table 3. The autocatalytic rate constant, k_α, is observed to increase with cure temperature, T_c, and also with UV light inten-

sity, I_{uv}. In fact, the temperature dependence of k_α is very well fitted with an Arrhenius equation as

$$k_\alpha = 9.22 \ \exp\left[-\frac{1105}{T_K}\right], \quad (r^2 = 0.994), \tag{14}$$

where T_K (K) denotes cure temperature in absolute scale and r^2 denotes the coefficient of determination (square of the correlation coefficient). This indicates the autocatalytic polymerization rate is enhanced at higher temperatures with an activation energy, $E_{a,\alpha}$, of about 1105R.

The rate constant for the initiation step, k_β, is also observed to increase with T_c and I_{uv}. The temperature dependence of k_β is relatively well fitted with an Arrhenius equation as

$$k_\beta = 24,400 \exp\left[-\frac{3305}{T_K}\right], \quad (r^2 = 0.952). \tag{15}$$

The activation energy for k_β is estimated to be $E_{a,\beta} = 3305R$, which is about three times larger than $E_{a,\alpha}$.

The rate constant for the decomposition of photoinitiators, k_γ, is estimated to decrease according to T_c and I_{uv}; however, the inverse dependence of k_γ on T_c and I_{uv} is only explained by the uncertainties in the measurement as well as in the parameter estimation. The conversion factor, m, is estimated to decrease with respect to T_c, but to remain relatively constant with respect to I_{uv}. The decrease of m at a higher cure temperature might be related to the increased consumption of primary radicals other than during the initiation step in Eq. (6), e.g. the primary radical termination [24].

5. Conclusion

The fast cure kinetics of a UV-curable resin designed for UV-NIL was studied by measuring the heat released during photopolymerization of the resin using DPC. The temporal evolution of degree of cure was determined by integrating the measured heat flow and then normalizing it by the total polymerization heat. A phenomenological kinetic model was formulated to describe the observed fast cure kinetics by considering the rate of change of the photoinitiator, γ, and the primary radical concentration, β, due to the production and initiation steps, and the rate of change of the degree of cure, α, due to the initiation step (α'_{pi}) and the propagation and termination steps (α'_{ac}). The phenomenological kinetic model was found to adequately describe the fast cure kinetics of the UV-curable resin considered in this study. The estimated kinetic model parameters were provided along with discussion on their dependence on cure temperature and UV light intensity. The phenomenological kinetic model proposed in this study is expected to be applicable to other UV-curable resins for UV-NIL, provided that a proper rate equation is used to describe the propagation and termination steps.

Acknowledgements

This work was supported by the Seoul R&BD Program (10583). The authors would like to thank the reviewers of this paper for their valuable comments.

References

[1] Y. Xia, J.A. Rogers, K.E. Paul, G.M. Whitesides, Chem. Rev. 99 (1999) 1823–1848.
[2] L.J. Guo, Adv. Mater. 19 (2007) 495–513.
[3] H. Schift, J. Vac. Sci. Technol. B 26 (2008) 458–480.
[4] C.M. Sotomayor Torres, Alternative Lithography: Unleashing the Potentials of Nanotechnology, Springer, New York, 2003.
[5] S.Y. Chou, P.R. Krauss, P.J. Renstrom, Appl. Phys. Lett. 67 (1995) 3114–3116.
[6] S.Y. Chou, P.R. Krauss, P.J. Renstrom, Science 272 (1996) 85–87.
[7] S.Y. Chou, P.R. Krauss, W. Zhang, L.J. Guo, L. Zhuang, J. Vac. Sci. Technol. B 15 (1997) 2897–2904.
[8] J. Haisma, M. Verheijen, K. van den Heuvel, J. van den Berg, J. Vac. Sci. Technol. B 14 (1996) 4124–4128.
[9] M. Bender, M. Otto, S. Altmeyer, B. Vratzov, B. Hadam, B. Spangenberg, H. Kurz, Microelectron. Eng. 53 (2000) 233–236.
[10] M. Colburn, S. Johnson, M. Stewart, S. Damle, T.C. Bailey, B. Choi, M. Wedlake, T. Michaelson, S.V. Sreenivasan, J.G. Ekerdt, C.G. Willson, Proc. SPIE 3676 (1999) 379–389.
[11] E. Andrzejewska, Prog. Polym. Sci. 26 (2001) 605–665.
[12] C. Decker, Macromol. Rapid Commun. 23 (2002) 1067–1093.
[13] S.C. Clark, C.E. Hoyle, S. Jonsson, F. Morel, C. Decker, Polymer 40 (1999) 5063–5072.
[14] I.V. Khudyakov, J.C. Legg, M.B. Purvis, B.J. Overton, Ind. Eng. Chem. Res. 38 (1999) 3353–3359.
[15] P. Kerbouc'h, P. Lebaudy, L. Lecamp, C. Bunel, Thermochim. Acta 410 (2004) 73–78.
[16] J.D. Cho, J.W. Hong, Eur. Polym. J. 41 (2005) 367–374.
[17] C.E. Corcione, M. Frigione, A. Maffezzoli, G. Malucelli, Eur. Polym. J. 44 (2008) 2010–2023.
[18] V.Y. Voytekunas, F.L. Ng, M.J.M. Abadie, Eur. Polym. J. 44 (2008) 3640–3649.
[19] G.B. Zhang, X.D. Fan, J. Kong, Y.Y. Liu, Polym. Bull. 60 (2008) 863–874.
[20] M.D. Dickey, R.L. Burns, E.K. Kim, S.C. Johnson, N.A. Stacey, C.G. Willson, AIChE J. 51 (2005) 2547–2555.
[21] M.D. Dickey, C.G. Willson, AIChE J. 52 (2005) 777–784.
[22] M. Vogler, S. Wiedenberg, M. Mühlberger, I. Bergmair, T. Glinsner, H. Schmidt, E.B. Kley, G. Grützner, Microelectron. Eng. 84 (2007) 984–988.
[23] G.R. Tryson, A.R. Shultz, J. Polym. Sci. Polym. Phys. Ed. 17 (1979) 2059–2075.
[24] M.D. Goodner, C.N. Bowman, Macromolecules 32 (1999) 6552–6559.